Considerations for temperature sensor placement on rotary-wing unmanned aircraft systems

Brian R. Greene[1,2,3], Antonio R. Segales[2,3,4], Sean Waugh[5], Simon Duthoit[2,3,4], and Phillip B. Chilson[1,2,3]

[1]University of Oklahoma School of Meteorology, Norman, Oklahoma
[2]Advanced Radar Research Center, University of Oklahoma, Norman, Oklahoma
[3]Center for Autonomous Sensing and Sampling, University of Oklahoma, Norman, Oklahoma
[4]University of Oklahoma School of Electrical and Computer Engineering, Norman, Oklahoma
[5]NOAA/OAR National Severe Storms Laboratory, Norman, Oklahoma

Correspondence: B. Greene (brian.greene@ou.edu)

Abstract. ~~With their recent surge in commercial accessibility,~~ Integrating sensors with a rotary-wing unmanned aircraft ~~systems~~ system (rwUAS) ~~are proving to be a viable method of atmospheric sensing and sampling while improving upon the shortcomings of traditional methods~~ can introduce several sources of biases and uncertainties if not properly accounted for. To maximize the potential for ~~these platforms~~ rwUAS to provide reliable observations, it is imperative to have an understanding of their strengths and limitations under varying environmental conditions. This study focuses on the quality of measurements relative to sensor locations on board rwUAS. Typically, thermistors require aspiration and proper siting free of heat sources to make representative measurements of the atmosphere. In an effort to characterize ideal locations for sensor placement, a series of experiments were conducted in the homogeneous environment of an indoor chamber with a pedestal-mounted rwUAS. A suite of thermistors along with a wind probe were mounted inside of a solar shield, which was affixed to a linear actuator arm. The actuator arm was configured such that the sensors within the solar shield would travel underneath the platform into and out of the propeller wash. The actuator arm was displaced horizontally underneath the platform while the motors were throttled to 50 percent, yielding a time series of temperature and wind speed which could be compared to temperatures being collected in the ambient environment. Results indicate that temperatures may be biased on the order of 0.5–1.0°C and vary appreciably without aspiration, sensors placed close to the tips of the rotors may experience biases due to frictional and compressional heating as a result of turbulent fluctuations, and sensors in proximity to motors may experience biases approaching 1°C. From these trials, it has been determined that sensor placement underneath a propeller on an rwUAS a distance of one quarter the length of the propeller from the tip is most likely to be minimally impacted from influences of turbulence and motor, compressional, and frictional heating while still maintaining adequate airflow. When opting to use rotor wash as a means for sensor aspiration, the user must be cognizant of these potential sources of platform-induced heating when determining sensor location.

1 Introduction

The planetary boundary layer (PBL) is the lowest layer of the troposphere which exchanges energy with the Earth's surface on timescales of less than one hour (Stull, 1988), and acquiring atmospheric measurements in this region has proven to be challenging ~~(Hardesty and Hoff, 2012). In the past, in-situ PBL measurements have been taken primarily with instrumented~~
5 ~~towers(e.g. Charba, 1974; Shapiro, 1984; Poulos et al., 2002), which are immobile and~~ (National Research Council, 2009; Hardesty and H PBL flows are highly complex and nonlinear in space and time, even with several layers of assumptions applied in theory. As such, it has always been a challenge for atmospheric scientists to collect representative measurements of the environment, even with continual advances in technology. One of the most common resources for PBL studies has been instrumented towers, which can continually provide data at a point location over long periods of time (e.g., Charba, 1974; Shapiro, 1984; Poulos et al., 2002).
10 While highly reliable and configurable, instrumented towers do come with an inherent downside. Being limited in vertical extent, ~~and balloons (e.g. Holden et al., 2000; Poulos et al., 2002; Seidel et al., 2010), which are costly and have limited vertical resolution. Furthermore,~~ the convective boundary layer often extends well above even the tallest of towers. Even networks with the 30 km average horizontal resolution of the Oklahoma Mesonet (Brock et al., 1995; McPherson et al., 2007) still cannot provide details on the vertical structure of the atmosphere.
15 Presently, weather balloons are the most common tool available for in-situ observations above the level of towers. They provide valuable kinematic and thermodynamic data from the upper atmosphere, which impacts both short-term weather forecasts (Cohen et al., 2007; Faccani et al., 2009; Lackmann, 2011) as well as climatological trends (Luers and Eskridge, 1998; Lanzante can serve as a baseline for model verification (Agustí-Panareda et al., 2010; Benjamin et al., 2010; Gensini et al., 2014). Rawinsondes are launched in hundreds of locations around the world every day, although usually only twice a day at most sites. This
20 operational network is also not suited to provide adequate PBL measurements, as they ascend too rapidly through the lowest levels (National Research Council, 2009). More frequent deployments with slower ascents are commonly performed on field campaigns (e.g., Kosiba et al., 2013; Parker, 2014; Trapp et al., 2016; Geerts et al., 2017), but this becomes expensive as the sensor package is rarely recovered for reuse. Specialized satellite remote sensors can derive vertical thermodynamic and kinematic profiles across significant areas of the Earth, but vertical resolutions in the PBL are too coarse for practical application.
25

Surface-based remote sensors such as wind profilers, ~~scanning~~ Doppler lidars, sodars, and radiometers are capable of continuously observing a fixed location ~~(e.g. Grund et al., 2001; Poulos et al., 2002; Banta et al., 2015; Bonin et al., 2015; Lundquist et al., 2017)~~ but rely on numerous assumptions about the atmosphere and have trouble resolving measurements close to the surface. These types of instruments are also cost-prohibitive when considering expansion to larger-scale networks such as the global upper-air
30 sites.
~~For several years now,~~ Even when combining surface towers, balloons, and remote sensors with other observational techniques such as tethered balloons, Doppler weather radars, and satellite remote sensors, the National Research Council (2009) still concluded that the "vertical component of U.S. mesoscale observations is inadequate." The NRC in this report implored

government agencies to pursue developments in capabilities to monitor the lower atmosphere at finer scales in space and time.

Capitalizing on the recent commercial accessibility of small unmanned aircraft systems (~~sUAS) , specifically fixed-wing UAS (fwUAS), have provided a unique ability to observe previously unattainable regions of the PBL both in space and time (Lothon et al., 2014; Wildmann et al., 2014; Båserud et al., 2016; de Boer et al., 2016; Bailey et al., 2017). Instrumentation on fwUAS has followed closely in the footsteps of operational~~ sUASs) and miniaturized sensor packages, numerous groups around the world have embraced the potential for integrated platforms to fill this atmospheric data void (e.g., Reuder et al., 2009; Houston et al., 20 UASs have the notable advantage of being able to operate in regions beyond the reach of typical systems, including environments that may be dangerous. Sophisticated systems can be deployed on a regular basis for consistent measurements, and they are less expensive alternatives to ground-based remote sensors measuring similar parameters. They can be used for a variety of missions measuring different quantities, such as horizontal transects across airmass boundaries or continuous vertical profiling at fixed ascent rates. Owing in part to the longstanding history of manned research aircraft, ~~and the body of literature regarding thermodynamic measurements has made these platforms a valuable resource (Saïd et al., 2005; Gioli et al., 2006; Reuder et al., 2012; van d~~ UASs (fwUASs) have been at the forefront of UAS development for atmospheric research (Saïd et al., 2005; Gioli et al., 2006; van den Kro However, ~~fwUAS~~ fwUASs come with several notable disadvantages, namely their inability to sample a vertical column at a fixed horizontal position, risks when operating close to the ground, and the need for a suitable surface for landing and possibly takeoff. Currently, rotary-wing ~~UAS (rwUAS~~UASs (rwUASs) are being ~~realized as~~ proven to be a viable supplement to ~~fwUAS~~ fwUASs thanks to their autonomous vertical takeoff/landing capabilities ~~and advancements in autopilot technology (Brosy et al., 2017; Vömel et al., 2018). The international network of operational radiosonde systems serve as the current standard for vertical profiling, and their observations are widely assimilated into numerical weather prediction. However, their limited spatio-temporal resolution is incapable of properly resolving PBL processes (National Research Council, 2009). As such, integration of rwUAS with~~ (Brosy et al., 2017; Vömel et al., 2018). Integration of rwUAS into observational networks and research efforts has the potential to vastly improve our understanding of processes occurring in the lowest regions of the atmosphere at unprecedented scales. It is therefore imperative for data collected by these platforms to achieve the highest possible degree of environmental representativeness as rwUAS become more commercially accessible.

As one application, rotary-wing UAS can be used to measure the same thermodynamic and kinematic properties as radiosondes: pressure, temperature, relative humidity, and horizontal wind speed and direction (Neumann and Bartholmai, 2015; Brosy et al., 2017). However, when making measurements, the platform itself can influence these observations. There are a number of factors that can affect any single measurement and each observation must be carefully designed and examined to ensure that it is as free as possible from external influence. In this study, we focus on the effects of sensor placement on temperature observations.

To ensure that a thermometer, such as a thermistor, produces accurate measurements, it is critical that the sensor be ~~well aspirated and properly mixed~~ shielded from solar radiation and properly aspirated with the ambient environment (Tanner et al., 1996; Richardson et al., 1999; Hubbard et al., 2004). Moreover, sensor self-heating can lead to significant measurement bias in some thermistors if not properly accounted for. Thermistors use a ~~temperature sensitive~~ temperature-sensitive resistor to

measure temperature. By knowing the input voltage and measuring how it changes across the thermistor, the resistance of the temperature sensitive resistor can be determined, and thus the air temperature. If current is run constantly through the resistor, heat is generated. Such a sensor must be properly aspirated or the resultant heat can modify the ambient environment, thereby influencing the measurement itself.

Observations of temperature from tower-mounted thermistors typically utilize solar-shielded chambers with fans to mechanically aspirate the sensors to improve data quality (Brock et al., 1995; McPherson et al., 2007). However, when considering the integration of sensors into a rwUAS, utilizing a fan poses a dilemma. Although a fan could ensure proper aspiration, ~~this~~ it would draw power and add weight to the platform and potentially significantly decrease flight duration. Therefore, an alternative solution to this problem ~~could be~~ is to aspirate the sensors with the air currents produced by the rotating propellers ~~, or rotor wash~~(i.e., rotor wash). However, due to the complex flow around a rwUAS in flight, the location on the rwUAS providing the best aspiration is not obvious. ~~Too little airflowand~~ If exposed to too little airflow, the sensor could self heat or not adequately sample the ambient atmosphere. ~~Too much airflowand~~ If exposed to too much airflow, compressional heating of the air stream becomes an issue (Rodert, 1941). Furthermore, ~~dissipation~~ emission of heat from the rotary motor can also alter the measured air. Flow in the proximity to the propeller tips is also associated with the highest values of turbulent intensity and temperature fluctuations (Swean and Schetz, 1979). After initial experiments involving rwUAS for research efforts, it was determined that a more in-depth examination of sensor location was needed to ensure data quality.

2 Equipment

With the questions surrounding temperature sensor placement on a rwUAS, an experiment was created to objectively determine the optimal location for quality temperature measurements, which is the primary focus of this study. ~~To accomplish the task, the placement of the sensors relative to the rwUAS~~ A summary of the findings from the experiment is discussed below.

2.1 Rotary-wing aircraft

The University of Oklahoma's custom-built CopterSonde rwUAS (Figure 1 facilitates a symmetrical carbon fiber hashtag design with a diameter of 65 cm and is driven by eight brushless electric motors and 25 cm diameter propellers. The maximum payload mass amounts to 1 kg with a total all-up weight of about 7 kg. The maximum flight time is about 20 minutes. The CopterSonde has a top flight speed of 25 m s^{-1} and thus can be flown safely in winds up to a maximum horizontal speed of 20 m s^{-1}. The CopterSonde is equipped with a Pixhawk autopilot (3D Robotics, Inc.) which relies on an on-board inertial measurement unit (IMU) for attitude estimation. A barometric pressure sensor is used to control the altitude of the rwUAS. It also carries a post-processing kinematic differential GPS unit which gives centimeter positioning accuracy in space. External sensor data are sent to the Pixhawk via the I^{2}C protocol, which are processed in parallel to the flight controls. This setup allows for a single consolidated data stream sent to the ground station over wireless radio using the Mavlink protocol. The operative distance of the communication system is around 5 km, capable of 15 km with upgraded antennas.

2.2 ~~InterMet temperature~~ Temperature sensors

~~To make temperature observations on the CopterSonde platform ,~~ The CopterSonde platform utilized PT 100 thermistors distributed by International Met Systems (iMet) ~~temperature sensors were used~~ to make temperature observations. These bead thermistors offer a response time of 2 seconds in still air (approximately 1 second with 5 m s^{-1} aspiration) over a range of -95 to +50°C, with an accuracy of $\pm$ 0.3°C and a resolution of 0.01°C. They are similar to the kind of sensors used on many standard radiosondes and ~~is~~ are ideal for use on a rwUAS. The sensors were ~~calibrated~~ validated using an Oklahoma Climatological Survey aspirated chamber located outside the National Weather Center in Norman, Oklahoma. Offsets for each sensor were determined over a period of several hours of a typical late afternoon in early spring, with temperatures comparable to room temperature. Thus, these offsets provide an implicit self-heating correction while aspirated.

The bead thermistors are one component of a bigger iMet system specifically designed for UAV applications: the iMet-XF UAV. This system uses a main board to which different types of thermodynamical sensors can be interfaced. It samples each connected sensor successively, including on-board GPS and pressure sensors, and provides these data in packets through serial communication. Acquiring and storing the data can be achieved in a variety of ways: using a pair of radios to stream data to a ground station, or the unit can be connected to a computer for direct data streaming using the provided iMet software.

On the CopterSonde, the iMet thermistors were utilized in conjunction with a custom data acquisition unit. These data were then streamed and recorded on a ground station computer using a radio frequency link. The iMet temperature sensors are equipped with an integrated circuit board that converts the analog data stream into an I^{2}C format. To streamline data input to the CopterSonde's flight controller (Pixhawk), a custom circuit board was developed that is capable of accepting and synchronizing 8 separate I^{2}C sensor inputs and converting them to a single output data stream. A module was programmed for the Pixhawk to sample each sensor successively at a given rate, log their data on-board, and stream live data to the ground station.

2.3 NSSL Mobile Mesonet

To provide a comparison with the temperature data recorded using the iMet thermistors, a modified version of the National Severe Storms Laboratory (NSSL) Mobile Mesonet (MM) rack was used. The equipment rack, normally mounted to the roof of a vehicle, is capable of temperature, pressure, wind speed and direction, relative humidity, and solar radiation observations. For the tests presented here, the equipment rack was mounted to a cart. This allowed the rack to be placed in close proximity to the CopterSonde during measurements.

To measure temperature, two ~~stainless steel probes from Campbell Scientific known as the~~ Campbell Scientific model 109 thermistors (CS 109) were used. One was mounted inside an aspirated radiation shield and one was mounted to the Copter-Sonde. The CS 109 has less than 0.03°C linearization error over the range of -50 to +70°C, with a $\pm$ 0.2°C tolerance between 0 and 70°C. The thermistor is contained within a stainless steel housing, meant for use in damp conditions such as soil moisture measurements, and as such has a response time of 30 s with 5 m s^{-1} airflow. The sensors used for this study had been recently calibrated ~~by the Oklahoma Climate Survey group and shown to be within specifications~~ in the Oklahoma Mesonet calibration lab to ensure its accuracy.

2.4 Oklahoma Mesonet hot-wire anemometer

In addition to measuring temperature, it is also relevant to measure the flow rate at the temperature sensor location. Doing so can indicate the extent to which the probes are in a "well mixed" environment and provides insight to the conditions that are being experienced by the sensors themselves. A Thermo Systems Inc. (TSI) hot-wire anemometer was used to gather precise velocity measurements about 1 cm from the temperature sensor mounting locations. On these scales, special considerations regarding the anemometer as a heat source were also required. As will be discussed in Section 4, a separate trial to control for possible interference was also conducted.

2.5 Linear actuator arm

The overall goal of the experiment was to find locations on a rwUAS where temperature readings are most representative of the environment. With this in mind, data collected at multiple locations on the rwUAS were examined to determine where the sensors experience bias relative to ambient air. To achieve this, the thermistors were placed on a linear actuator arm capable of moving the sensors horizontally directly underneath two of the motor mounts, as depicted in Figure 2. The initial starting position at point A was 6.5 cm outside of one propeller, and the the sensor position was systematically stepped 0.24 cm per increment with a dwelling time of two seconds per increment across the width of the CopterSonde towards point B. This motion of the arm was controlled by the same procedure on the ground station communicating with the hot-wire anemometer, which then recorded arm position, wind speeds, and computer timestamps at each step. The ending location was 12.5 cm outside the opposite side of the rwUAS, and took approximately 35 minutes to complete the process. Two of the iMet temperature sensors were attached to the arm, as was a 109 temperature sensor from the NSSL MM rack. Combining these three different datasets (NSSL logs for the NSSL probes, Pixhawk logs for the temperature sensors, and the computer logs for the arm and the anemometer) with their common timestamps therefore allowed for synchronized analysis of the separate data streams.

3 Thermistor self-heating experiment

Prior to analysis of the sensor placements (detailed in Sections 4 and 5), a baseline characterization of the iMet thermistor self-heating is required. A simple experiment consisting of three thermistors and a ducted fan was conducted to isolate the effects of aspiration. The fan was located at the base of a solar shield duct, which was bent at a right angle with sensors inserted through holes along the top. With the fan switched on, this configuration induced airflow to enter from the horizontal, pass across the sensors, and exhaust downwards through the fan.

The sensors were initially powered on to collect data while the fan was off. After holding this condition for approximately six minutes, the fan was powered on, pulling air across the sensors at 6 m s^{-1}. The fan was then alternately switched on and off for periods of two to three minutes each, for a total of three cycles.

~~A time series~~ Analysis of the iMet temperature responses ~~are displayed in Figure 3, along with green and red dashed lines denoting the times the fan was switched on and off, respectively. The data presented are the raw, uncalibrated output at 10 Hz. Although they are uncalibrated, the sensors closely track~~ (Figure 3) revealed that the sensors closely tracked with one another while the fan ~~is on~~ ~~and are only linearly~~ was on, with only a linear offset. It is immediately apparent that the sensors react to airflow through the solar shield, as temperatures repeatedly drop over 1°C in under 20 ~~seconds.~~ s. The temperature increase observed in all three sensors around minute 8 is due to a researcher stepping in front of the setup to take a photograph. While small, the aspirated sensors were capable of picking up on the influence of body heat and respond in a similar fashion. Prior to the first time the fan was switched on, the setup ~~had been sitting idly~~ was idle for several minutes. However, following the fan being switched off, the sensors indicated temperature increases. For these periods, the observed heating was likely due to a combination of both sensor-self heating and the fan motor radiating heat upwards towards the sensors. This hypothesis is supported by iMet sensor 2 being in closest proximity to and directly above the fan while also heating the most rapidly. Furthermore, the other two sensors were higher up and displaced horizontally due to the geometry of the duct, and they showed slower heating rates while the fan was off. The key evidence for sensor self-heating is that the sensors return to their same respective temperature levels each time the fan was on, regardless of how they behaved while the fan was off. Therefore, this supports the requirement of sensor aspiration to properly measure the environmental temperature.

4 Anechoic chamber experiments

4.1 Setup

The University of Oklahoma Radar Innovations Laboratory has a large anechoic chamber used for calibration and testing of radar components and other electronic equipment. This chamber~~however~~, however, also provides a reasonably homogeneous environment for testing when it is necessary to isolate the effects of various sensor influences on a rwUAS without solar radiation concerns or changes to the ambient environment. To offset the vertical variations in temperature that could exist in such a room, a common carpet fan was aimed at 45° from horizontal and turned on to maximum airflow about 15 minutes before the experiment to mix the ~~environment~~environmental air. The CopterSonde was mounted on a large pedestal near the center of the room with a bracket that accommodated the vehicle and a linear actuator arm as previously mentioned (Figure 4~~a~~A).

To simulate the wind flow of the aircraft in flight, the iMet and ~~NSSL thermistors and Mesonet wind probe~~ CS 109 thermistors and hot-wire anemometer were positioned inside of a 3D-printed plastic solar shield (Figure 4~~b, c~~B, C). Due to the spatial constraints of the setup, the ~~NSSL probe~~ CS 109 was mounted vertically and underneath the iMet and wind sensors in an effort to measure the same air stream. Furthermore, to avoid bias in ~~temperatures measured from the NSSL probe beneath the hot wire anemometer, the wind probe~~ temperature measurements, the hot-wire anemometer was removed for the final round of testing.

For each experiment, the actuator arm was mounted so that the sensors would pass directly underneath the motor mounts as the linear actuator arm moved horizontally ~~. Relative positions of each sensor to the rwUAS are detailed in Figure 2~~(Figure 2).

To provide a reference ~~background~~ temperature of the ambient environment, a second 109 sensor on the NSSL MM rack was mounted inside the aspirated U-tube radiation shield ~~(not depicted)~~(not depicted, see Waugh and Fredrickson, 2010). A second iMet thermistor was also suspended 50 cm below the CopterSonde, allowing for reasonable (but turbulent) aspiration, as determined from previous trials not included in this study. The additional measurements provided by the suspended iMet thermistor and the ~~NSSL MM~~ CS 109 probe inside the radiation shield, were used to ~~identify the "~~measure the "ambient" environment. For the purposes of these tests, the autopilot inputs to the motor throttle were bypassed, allowing for direct manipulation of throttle input using an external device.

4.2 Procedure

~~Upon receiving power,~~ To begin, power was supplied to the iMet and NSSL thermistors ~~and they~~ began logging data. For the first trial, the motor position began at point A (6.5 cm horizontally from the tip of the nearest propeller, ~~figure~~ Figure 2), and the battery was connected with throttle at zero, allowing the sensors to ~~record unaspirated~~ sample an unaspirated environment for 8 minutes. After this period, the CopterSonde was throttled up to approximately 55 percent maximum power to simulate the airflow typical during slow ascent. Although not directly under the propellers, airflow across the sensors was 2 m s^{-1}, sufficient enough for aspiration. This position was sustained for 2 minutes before powering the motors off again. The sensors then remained in quiescent conditions for 2.5 minutes before throttling to 55 percent again. After giving the sensors 40 seconds to aspirate, the linear actuator was then incrementally moved towards point B by 0.24 centimeters, holding each position for 2 seconds. In total, it moved approximately 71.1 cm, which was outside of the rotor wash on the "B" side of the configuration. This experiment took a total of approximately 35 minutes to complete.

To control for the effects of potential heat advection from the ~~hot-wire~~ hot wire anemometer, the same test was conducted after removing ~~the wind probe~~ it from the solar shield. During this second trial, however, the initial start-stop-start of the motors was not performed. The CopterSonde and sensors were powered on for 2.7 minutes, then the throttle was increased to 55 percent for 35 seconds before incrementing the linear actuator arm's position.

5 Results and discussion

5.1 Experiment 1 - wind probe in tube

~~Temperature and velocity are plotted versus relative time as the sensors moved along the linear actuator arm during the first experiment~~in Figure 5. ~~To~~ In the first experiment, to account for the longer response function of the ~~NSSL~~ CS 109 probes and to make more appropriate comparisons, a moving ~~boxcar~~ 10 s average of the iMet ~~temperatures was applied to 10 seconds~~ temperature data was calculated before each analysis point ~~; wind speeds displayed~~ (Figure 5). The wind speeds presented are the raw ~~output~~outputs. Furthermore, the hot-wire anemometer had not been calibrated prior to this experiment, and thus values displayed may not be absolute~~; however, confidence~~. Confidence in relative precision is still high~~.~~

~~In figure 5, the background temperature is shown by the NSSL 109 probe (dotted black) and the iMet sensor (solid black). The CopterSonde temperatures are shown by the iMet sensor (solid blue), while the reference temperature of the NSSL 109 is shown in solid red. The figure also shows the air velocity at the CopterSonde sensor location (solid orange), showing clear signs of passing~~, however.

The air flow velocity peaked near 17 m s^{-1} before decreasing to near zero directly underneath the motor which clearly identified passage through the rotor wash of the propellers as the linear actuator moves from one side of the rwUAS to the other ~~. This is indicated by peaks in the velocity as the hot-wire approached 17 m s^{-1} flow rates, before decreasing to near zero directly underneath the motor~~(points B, D, Figure 2). A second minimum was encountered between the two propellers, before a similar pattern was observed while the sensors passed under the second propeller. A gradual temperature increase of 0.5° ~~C~~ was observed by both background temperature sensors over the course of the 35 ~~minute~~ min experiment, likely attributable to the mechanical mixing of the chamber environment.

This velocity pattern and associated temperature bias demonstrates that when considering sensor location for adequate airflow, directly under the motors or between the two propellers is not a viable option. While the first conclusion might be obvious, a relative minima in the flow velocity was not expected between the propellers. In addition~~to the velocity structure, Figure 5 shows that~~, differences do exist between the various sensors, and ~~that~~ a steady increase in temperature on all sensors was measured over the duration of the experiment ~~.~~(Figure 5). To account for this steady increase, temperatures relative to the background environment are considered for the remainder of this discussion.

A closer look at the first 16 minutes of this analysis relative to the background temperature (Figure 6) reveals evidence of the self-heating phenomenon. For over 8 minutes, the probes in the solar shield recorded 0.2–0.4°C above the relatively constant background, with variations owing to the presence of the hot-wire anemometer. During this period, the motors of the CopterSonde were not on, thus no aspiration to the sensor existed. Once the motors initially throttled up (green dashed line), temperatures dropped to within 0.1°C of the reference, and remained in this range until the motors were shut off again 2 minutes later. Immediately after throttling down, temperature began rising again, by 0.5°C in under 3 minutes. Finally, when throttled back up again at the 13 minute mark, temperatures returned to anomalies of 0.1°C in under 30 seconds.

Although influences from the anemometer are likely inherent during this initial period, the overall response of the sensors to aspiration matches results from the experiment discussed in ~~section 3.~~ Section 3. It can therefore be concluded that rotor wash is capable of mitigating the decoupling of sensors from the ambient environment, so long as the sensors are free from other external sources of heating which will be discussed below.

After the motors turned on at the 13-minute mark, the actuator arm began translating underneath the aircraft. Due to the complexity of the flow field underneath propellers rotating at several thousand revolutions per minute, it is reasonable to believe that small nuances in temperature depicted can be caused by limits in sensor accuracy and sampling rates in turbulent flow. There are, however, several identifiable trends that are attributable to artificial sources such as motor heat and sensor decoupling (Figure 7).

At minute 15.5 (just prior to point B), the probes intercepted a warm stream of air likely owing to turbulent fluctuations and compressional heating on the tip of the propeller spreading down and outward along the periphery of the propeller wash.

A similar observation is made on the other end of the CopterSonde at minute ~~28.~~28 (after point H). At minute 16 (point B), the sensors moved under the propellers and out of the warm air stream from the tips, allowing temperatures to stabilize within ~~0.1~~0.2°C of the reference temperature. This pattern is consistently observed underneath the four peaks in wind speed, representing: exterior propeller 1 (point B), interior propeller 1 (point D), interior propeller 2 (point F), and exterior propeller 2 (point H), in order.

As the actuator arm moved the sensors underneath the CopterSonde's motor mounts from minutes 18–19.5 (point C) and 25–26.5 (point G), temperatures rapidly rose ~~0.5–0.8~~0.7–1.0°C relative to the background over the course of 1 minute (Figure 7). Since temperatures began rising with wind speeds well above levels at the beginning of the experiment (2–4 m s^{-1}), the source of this increase was not necessarily solely due to self heating. Instead, their proximity to the motors leads to the conclusion that the sensors were intercepting hot air ~~streaming off~~advected from the motors.

Finally, the sensors mounted on the arm sampled the space in between the interior propeller tips at minutes 21.5~~-23. Wind~~–23 (point E). At that time, wind speeds dropped to ~~marginal levels~~less than 3 m s^{-1}, similar to those at the initial position of the sensors. Subsequently, a small (0.1°C) temperature rise is noted in both the iMet and NSSL sensors. Because the aspiration rates were similar to those at the beginning of this experiment, the primary driver of this temperature rise was likely a combination of self-heating and intercepting a warm air stream originating from the ~~hot wire~~hot-wire anemometer. In order to ~~remove this effect~~account for the influence of the hot-wire anemometer, a second analogous experiment was performed by removing ~~the wind probe~~it.

5.2 Experiment 2 - no wind probe

In ~~the repeated experiment~~Experiment 2, sensors were allowed to remain unaspirated for about 2.75 ~~minutes~~min before throttling up and moving the linear actuator arm, similar to ~~experiment~~Experiment 1 except without the initial aspiration test. Although the wind probe was removed, the actuator arm increments were identical, so it is reasonable to compare the temperature time series against the wind speeds from ~~experiment~~Experiment 1 ~~are plotted in Figure 8for reference~~(Figure 8). In general, the temperature pattern was largely similar to the results from ~~experiment~~Experiment 1: symmetrical about the center of the two propellers, increases in temperature on the outside tips (before point B and after point H), and large increases underneath the motor mounts (points C and G). However, the small rise in temperature in between both propellers (point E) was no longer observed, and the overall increase in temperature underneath the motor mounts was ~~0.1-0.2 °C~~0.2–0.3°C less than in ~~experiment~~Experiment 1. Therefore, the hot-wire anemometer ~~was likely biasing~~likely biased temperature readings in this region of relatively stagnant flow.

Finally, the CopterSonde's battery rapidly approached ~~critical~~its critical level as the motors were shut off at ~~minute~~min 18.5, so temperature trends after this mark should not be strongly considered.

6 Conclusions

One must take special consideration regarding sensor placement when attempting to measure environmental temperature using a rotary-wing UAS because these platforms are prone to modifying their own environments. In order to determine sensor locations free of systematic biases, multiple experiments were conducted in a relatively homogeneous chamber, where sensors were sequentially displaced underneath the rotor wash from a mounted rwUAS. Results from the two experiments presented ~~, as well as other trials not described,~~ provide useful guidelines with regards to sensor placement. Several sources of temperature bias exist, including (but not limited to) those observed in this study: sensor self-heating, compressional heating and turbulent fluctuations from the propeller-modified air streams, and heating from the motors.

In addition to the two experiments discussed previously, several test trials were also conducted. These additional experiments were almost identical to the setup described in Section 4, but were missing some key elements. For instance, the sensors were mounted to the linear actuator arm without a solar radiation shield. As a result, the sensors intercepted larger areas of influence from heat sources such as the motors and propeller tips when compared to sensors inside a shield. Furthermore, the environmental air was not mixed using a carpet fan prior to running the experiment. There was a much more noticeable increase in the chamber's background temperature during these trials, which reduced confidence in analysis and was difficult to reproduce. These tests ultimately still eluded to similar results in temperature sensor placement, prompting the more refined experiments as the focus of this study.

Given these results, out of the locations tested the optimal position for measuring environmental temperatures while hovering or ascending with a rotary-wing UAS is in a solar shield about 5–10 cm below the propeller and one third the length of the propeller from the tip. This location provides ample aspiration while avoiding the warm air streams from the motor and propeller tips. Other locations above or below the UAS run the risk of encountering stagnation in flow, which can exaggerate the effects of self-heating and generally decouple the sensor from the environment. Furthermore, proximity to external heat sources such as batteries or the rotary motors are also capable of introducing artificially warmed air streams. By following these general guidelines, it is of the authors' opinions that rwUAS are capable of obtaining trustworthy atmospheric measurements across a variety of applications.

Figure 1. The CopterSonde, an octo-rotor UAS designed and built by the Center for Autonomous Sensing and Sampling at the University of Oklahoma.
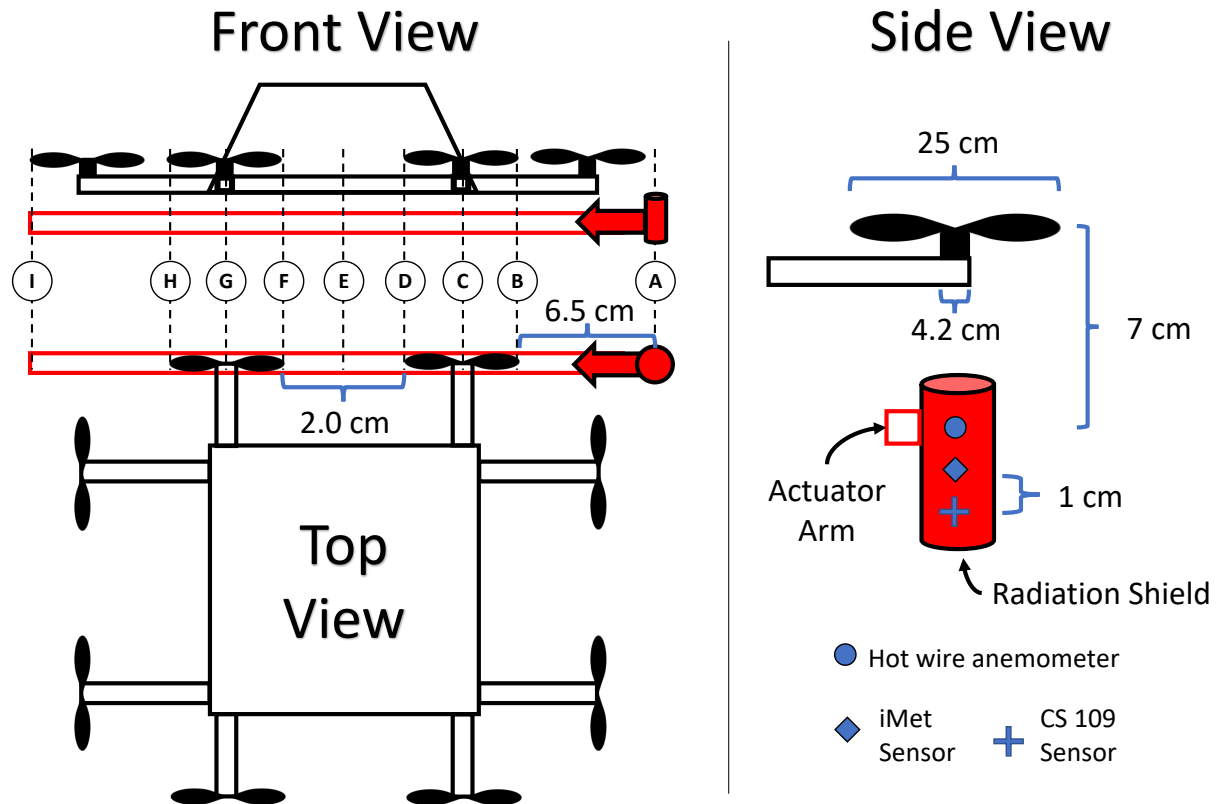
Figure 2. ~~Setup schematic~~ Schematic and dimensions of the rwUAS used in this study (drawing not to scale). In front and top view, the linear actuator arm is represented by the red rectangle outline, and the sensor package as a red circle. The arm was displaced from point A to point ~~B~~I, directly underneath the motor mounts and one pair of propellers as seen in the top-down and side views. Point B represents the tip of propeller 1, point C is directly under motor 1, D is the other side of the same propeller. Point E is halfway between the two propellers, and points F–H are symmetrical to points B–D.
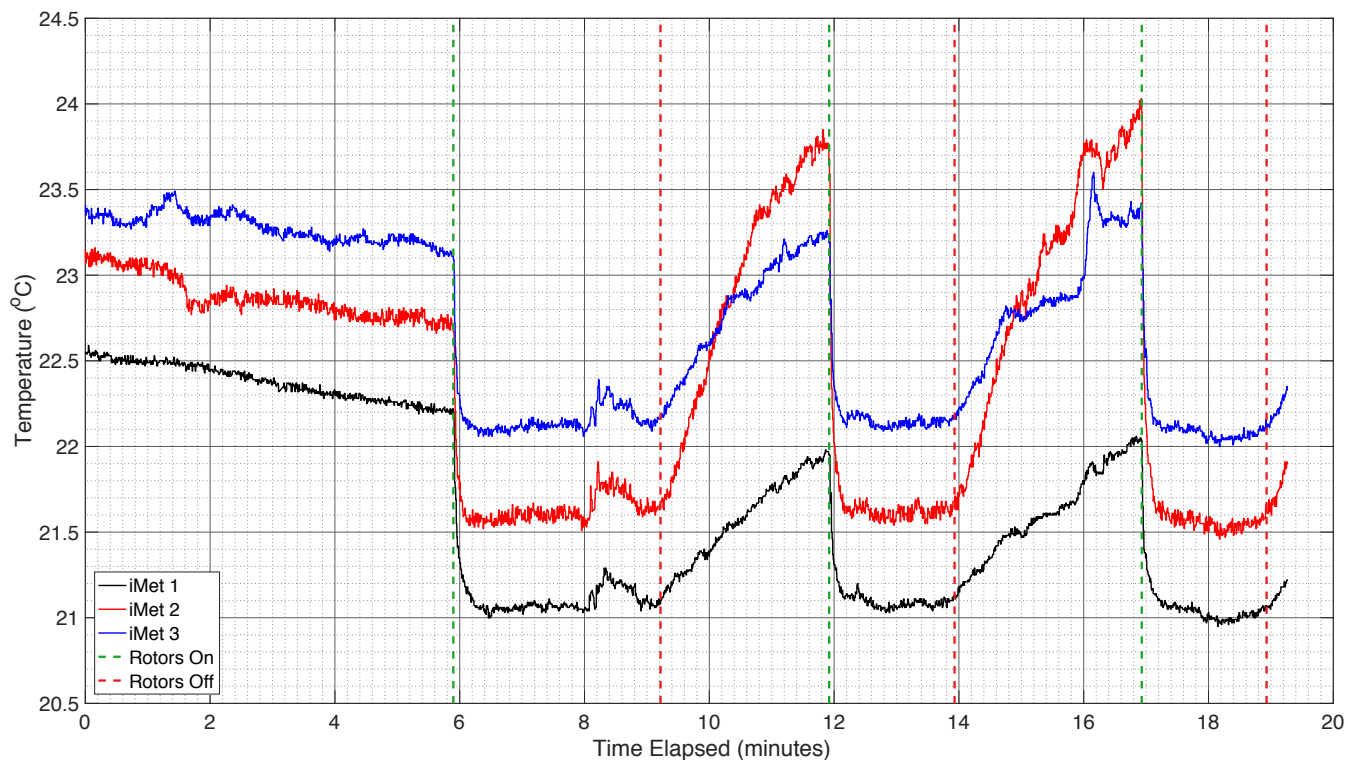
Figure 3. ~~Sensor aspiration experiment identifying sensor self-heating. After~~ Time series of the uncalibrated iMet temperature sensors sampling at 10 Hz relative to the times the fan ~~is~~ was switched on ~~initially~~ (green dashed line) ~~, temperatures drop over 1°C in response to coupling with the ambient environment. Each time the fan turns~~ and off (red dashed ~~lines~~line) ~~, temperatures rise as a result of self-heating and the fan radiating heat.~~ ~~Temperatures return to the same levels each time the fan is turned on, indicating proper sampling of the environment when aspirated.~~
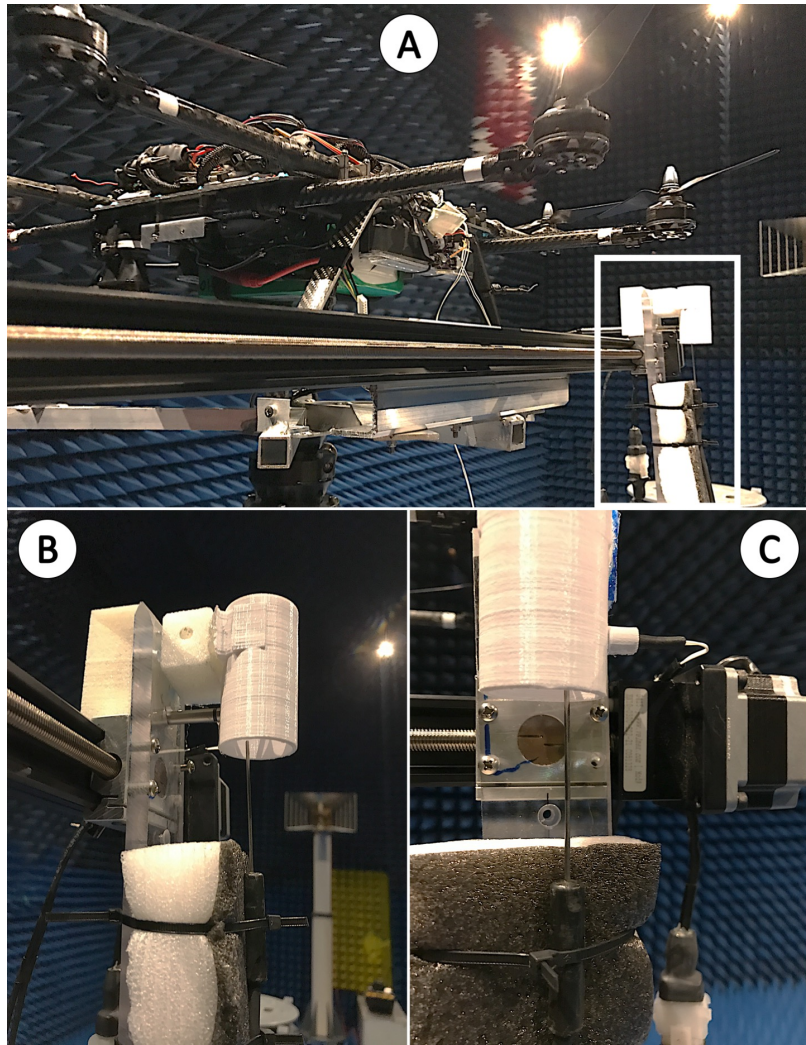
Figure 4. ~~a~~A: Position of linear actuator arm underneath rwUAS on mounting pedestal. Arm was aligned such that sensors passed directly underneath the motor mounts so as to make the system essentially two-dimensional. ~~b, c~~The sensor package is outlined in white. B: Close-up side view of the sensor package. The NSSL thermistor (CS 109) is strapped vertically to a foam mount so that it reaches inside the solar shield (white cylinder) from the bottom. ~~Location~~ The hot-wire anemometer is attached to the linear actuator arm with a clear mount and passes into a hole on the back side of the solar shield. C: Close-up front view of the sensor package. An iMet thermistor ~~, Mesonet wind probe, and NSSL thermistor inside~~ (PT 100) enters the solar shield through a hole on the right side. CS 109 also visible pointing vertically.
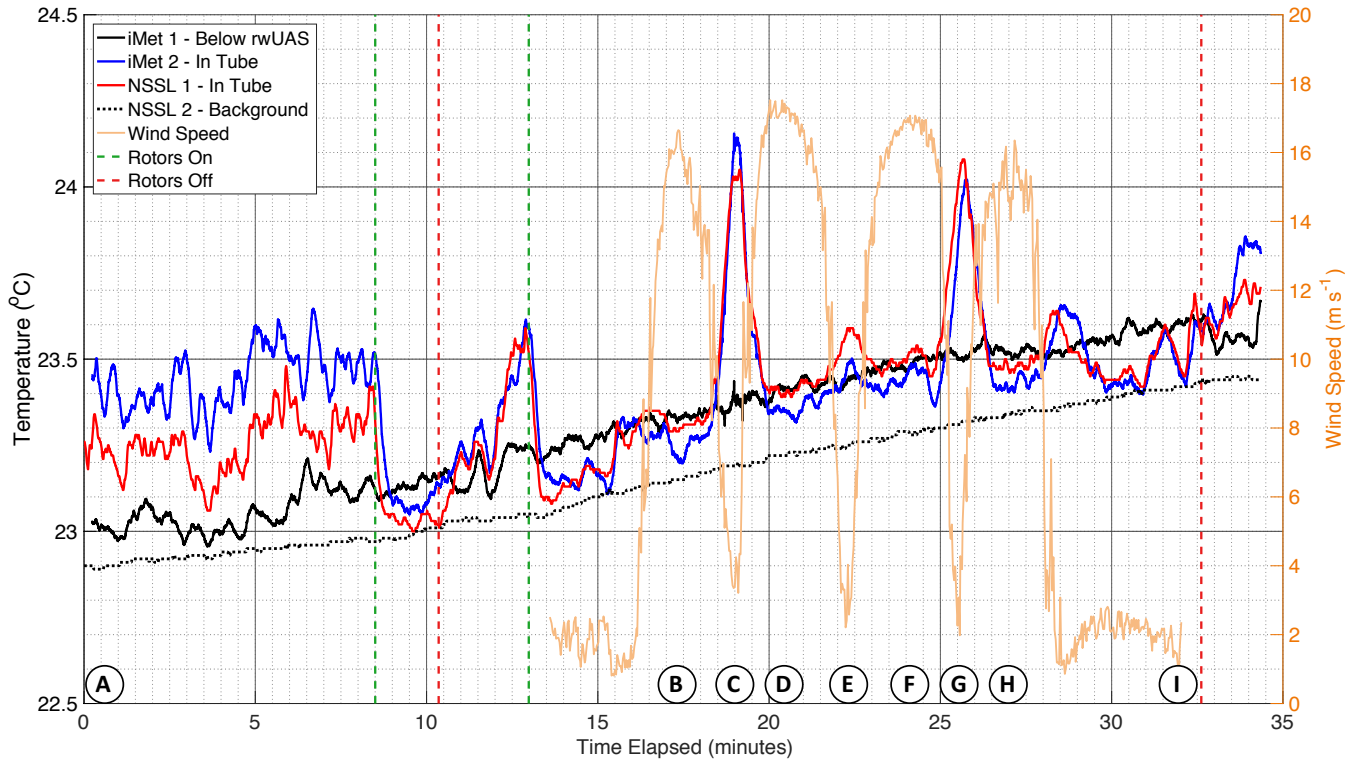
Figure 5. Experiment 1 - ~~Time series graph of air~~ temperature ($^\circ$C) and wind speed ~~vs~~(m s^{-1}). ~~relative time, entire time series~~The background temperature is shown by the CS 109 probe (dotted black) and the iMet sensor (solid black). ~~Temperature response to aspiration noticeable between minutes 8.3–10.3. Compressional heating off tip~~ The CopterSonde temperatures are shown by the iMet sensor (solid blue), while the reference temperature of ~~propeller at minute 15.5 just as wind speed picks up. Rise~~ the CS 109 is shown in ~~temperature underneath motor mount~~ solid red. Air velocity at ~~minute 19. Small rise~~ the CopterSonde sensor location is plotted in ~~temperature between two propellers at minute 22.3 due to hot wire anemometer in stagnant air~~solid orange. ~~Same pattern reflected for second half due to symmetry of setup~~Dotted green and red vertical lines indicate times when the motors were throttled on and off, respectively. Points A–I from Figure 2 are also indicated here.
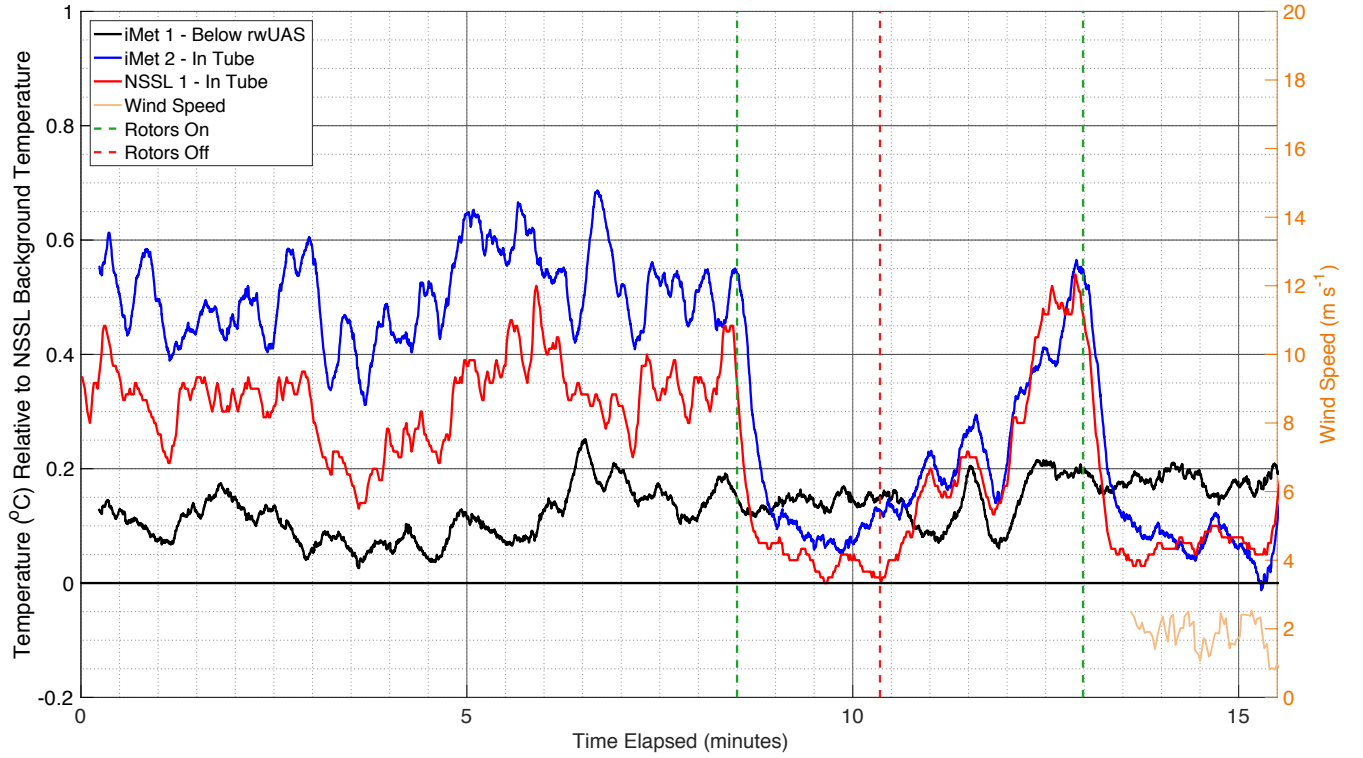
Figure 6. Temperatures ($^\circ$C) relative to NSSL background temperature at the beginning of ~~experiment~~ Experiment 1. This perspective emphasizes sensor self-heating (in addition to bias from the ~~hot wire~~ hot-wire anemometer) as the propellers are throttled on and off (green and red vertical dashed lines, respectively). Furthermore, the initial difference between NSSL sensors can be attributed to the presence of the anemometer in the radiation shield. While wind speeds were not recorded during this time, it is reasonable to extrapolate the 2.5 m s^{-1} reading backwards from minute 13.6 since the sensor position was fixed.
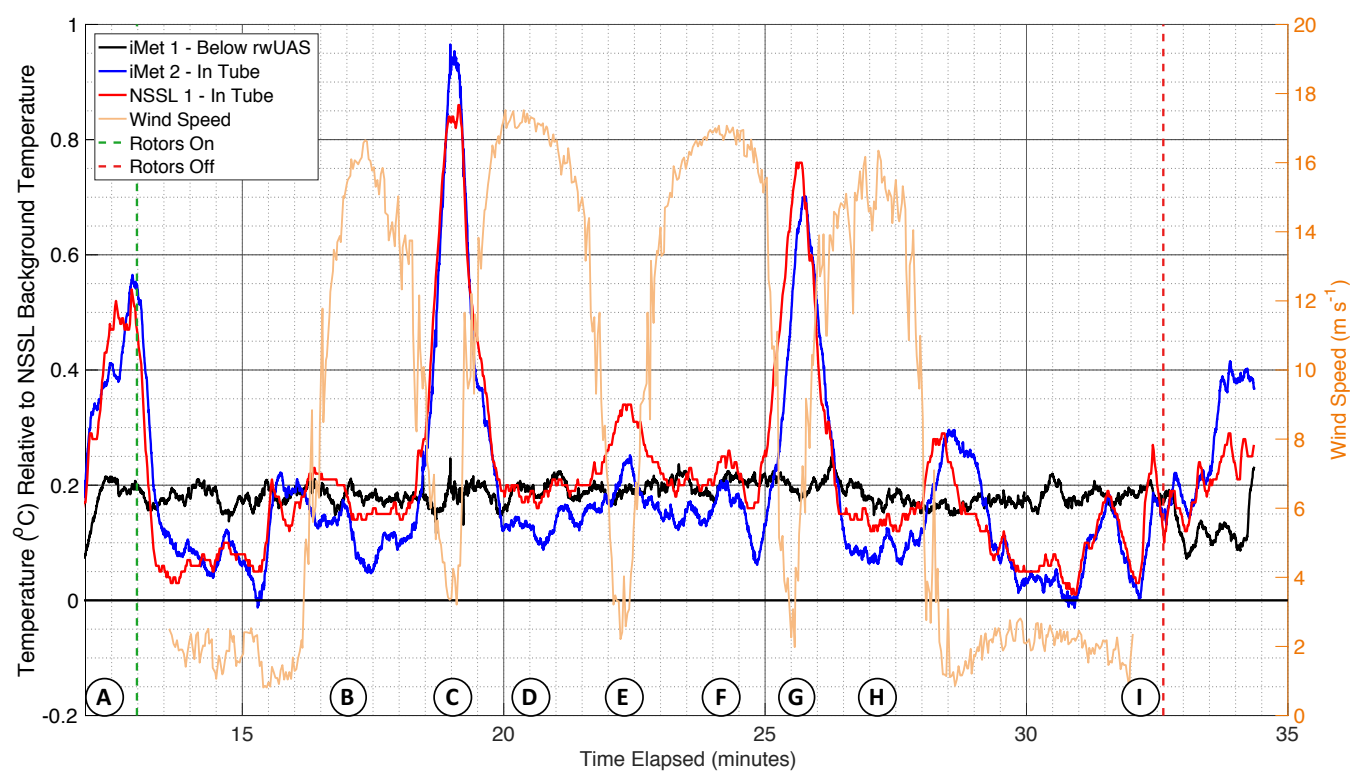
Figure 7. Experiment 1 time series of temperature (°C) relative to the NSSL background temperature after the actuator arm begins incrementing. Points A–I are included from Figure 2.
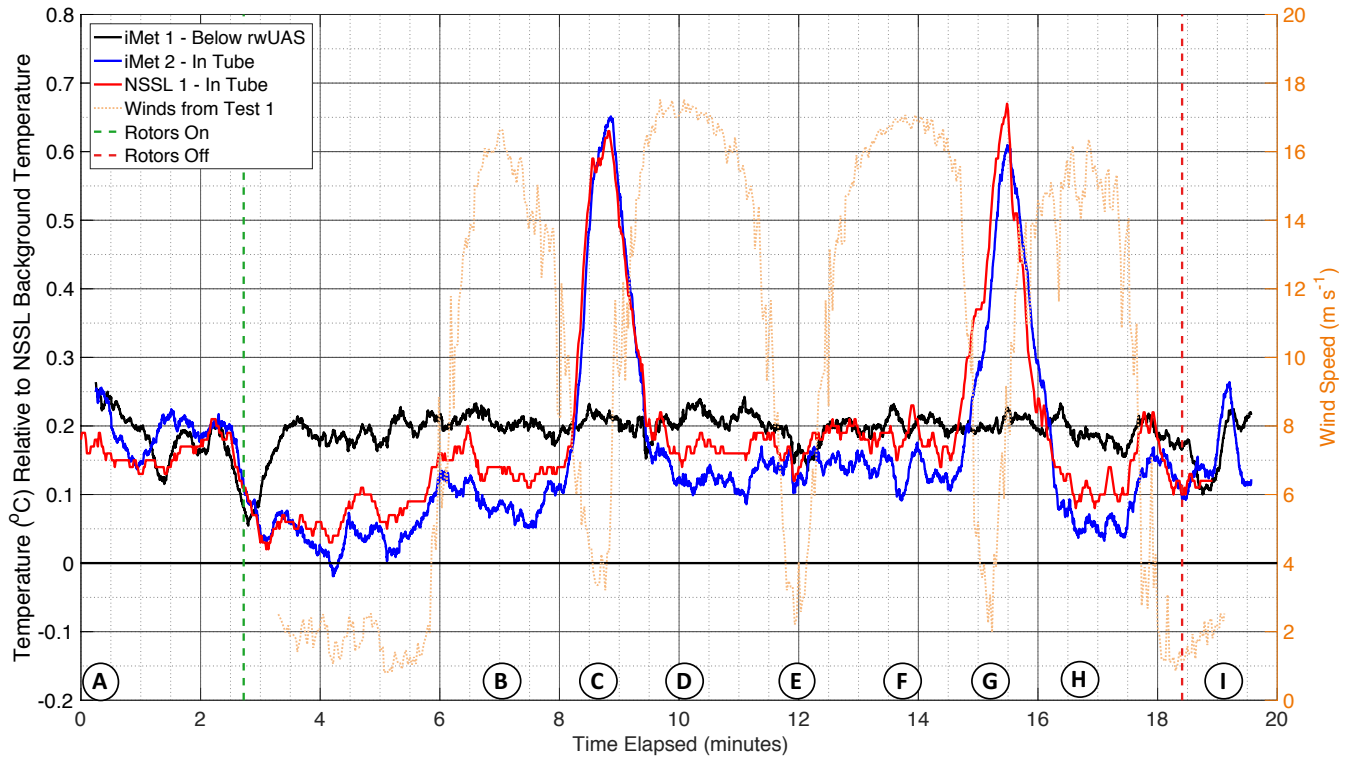
Figure 8. Experiment 2 - temperature and wind speed vs. relative time. Winds from ~~experiment~~ Experiment 1 included for reference (dotted orange). ~~Results~~ Points A–I are ~~similar to experiment 1, but the lack of small temperature rises in between the propellers indicates that the hot wire anemometer was modifying air streams to an extent~~ included from Figure 2. ~~Therefore, this is a more characteristic depiction of an rwUAS in flight.~~

Competing interests. The authors declare that they have no conflicts of interest.

References

Agustí-Panareda, A., Beljaars, A., Cardinali, C., Genkova, I., and Thorncroft, C.: Impacts of Assimilating AMMA Soundings on ECMWF Analyses and Forecasts, Weather and Forecasting, 25, 1142–1160, https://doi.org/10.1175/2010WAF2222370.1, 2010.

Bailey, S. C. C., Witte, B. M., Schlagenhauf, C., Greene, B. R., and Chilson, P. B.: Measurement of High Reynolds Number Turbulence in the Atmospheric Boundary Layer Using Unmanned Aerial Vehicles, vol. 10, International Symposium on Turbulence and Shear Flow Phenomena, 2017.

Banta, R. M., Pichugina, Y. L., Brewer, W. A., Lundquist, J. K., Kelley, N. D., Sandberg, S. P., Alvarez II, R. J., Hardesty, R. M., and Weickmann, A. M.: 3D volumetric analysis of wind turbine wake properties in the atmosphere using high-resolution Doppler lidar, J. Atmos. Ocean. Tech., 32, 904–914, https://doi.org/10.1175/JTECH-D-14-00078.1, 2015.

Båserud, L., Reuder, J., Jonassen, M. O., Kral, S. T., Paskyabi, M. B., and Lothon, M.: Proof of concept for turbulence measurements with the RPAS SUMO during the BLLAST campaign, Atmos. Meas. Tech., 9, 4901, https://doi.org/10.5194/amt-9-4901-2016, 2016.

Benjamin, S. G., Jamison, B. D., Moninger, W. R., Sahm, S. R., Schwartz, B. E., and Schlatter, T. W.: Relative Short-Range Forecast Impact from Aircraft, Profiler, Radiosonde, VAD, GPS-PW, METAR, and Mesonet Observations via the RUC Hourly Assimilation Cycle, Monthly Weather Review, 138, 1319–1343, https://doi.org/10.1175/2009MWR3097.1, 2010.

Blumberg, W. G., Wagner, T. J., Turner, D. D., and J. Correia, J.: Quantifying the Accuracy and Uncertainty of Diurnal Thermodynamic Profiles and Convection Indices Derived from the Atmospheric Emitted Radiance Interferometer, Journal of Applied Meteorology and Climatology, 56, 2747–2766, https://doi.org/10.1175/JAMC-D-17-0036.1, 2017.

Bonin, T. A., Blumberg, W. G., Klein, P. M., and Chilson, P. B.: Thermodynamic and turbulence characteristics of the southern great plains nocturnal boundary layer under differing turbulent regimes, Bound.-Lay. Meteorol., 157, 401–420, https://doi.org/10.1007/s10546-015-0072-2, 2015.

Brock, F. V., Crawford, K. C., Elliott, R. L., Cuperus, G. W., Stadler, S. J., Johnson, H. L., and Eilts, M. D.: The Oklahoma Mesonet: a technical overview, J. Atmos. Ocean. Tech., 12, 5–19, https://doi.org/10.1175/1520-0426(1995)012<0005:TOMATO>2.0.CO;2, 1995.

Brosy, C., Krampf, K., Zeeman, M., Wolf, B., Junkermann, W., Schäfer, K., Emeis, S., and Kunstmann, H.: Simultaneous multicopter-based air sampling and sensing of meteorological variables, Atmos. Meas. Tech., 10, 2773–2784, https://doi.org/10.5194/amt-10-2773-2017, 2017.

Charba, J.: Application of gravity current model to analysis of squall-line gust front, Mon. Weather Rev., 102, 140–156, https://doi.org/10.1175/1520-0493(1974)102<0140:AOGCMT>2.0.CO;2, 1974.

Cohen, A. E., Coniglio, M. C., Corfidi, S. F., and Corfidi, S. J.: Discrimination of Mesoscale Convective System Environments Using Sounding Observations, Weather and Forecasting, 22, 1045–1062, https://doi.org/10.1175/WAF1040.1, 2007.

de Boer, G., Palo, S., Argrow, B., LoDolce, G., Mack, J., Gao, R.-S., Telg, H., Trussel, C., Fromm, J., Long, C. N., Bland, G., Maslanik, J., Schmid, B., and Hock, T.: The Pilatus unmanned aircraft system for lower atmospheric research, Atmos. Meas. Tech., 9, 1845–1857, https://doi.org/10.5194/amt-9-1845-2016, 2016.

Faccani, C., Rabier, F., Fourrié, N., Agusti-Panareda, A., Karbou, F., Moll, P., Lafore, J.-P., Nuret, M., Hdidou, F., and Bock, O.: The Impacts of AMMA Radiosonde Data on the French Global Assimilation and Forecast System, Weather and Forecasting, 24, 1268–1286, https://doi.org/10.1175/2009WAF2222237.1, 2009.

Geerts, B., Parsons, D., Ziegler, C. L., Weckwerth, T. M., Biggerstaff, M. I., Clark, R. D., Coniglio, M. C., Demoz, B. B., Ferrare, R. A., Jr., W. A. G., Haghi, K., Hanesiak, J. M., Klein, P. M., Knupp, K. R., Kosiba, K., McFarquhar, G. M., Moore, J. A., Nehrir, A. R., Parker, M. D.,

Pinto, J. O., Rauber, R. M., Schumacher, R. S., Turner, D. D., Wang, Q., Wang, X., Wang, Z., and Wurman, J.: The 2015 Plains Elevated Convection at Night Field Project, Bulletin of the American Meteorological Society, 98, 767–786, https://doi.org/10.1175/BAMS-D-15-00257.1, 2017.

Gensini, V. A., Mote, T. L., and Brooks, H. E.: Severe-Thunderstorm Reanalysis Environments and Collocated Radiosonde Observations, Journal of Applied Meteorology and Climatology, 53, 742–751, https://doi.org/10.1175/JAMC-D-13-0263.1, 2014.

Gioli, B., Miglietta, F., Vaccari, F. P., Zaldei, A., and De Martino, B.: The Sky Arrow ERA, an innovative airborne platform to monitor mass, momentum and energy exchange of ecosystems, Ann. Geophys.-Italy, 49, http://www.ann-geophys.net/49/109/2006/, 2006.

Grund, C. J., Banta, R. M., George, J. L., Howell, J. N., Post, M. J., Richter, R. A., and Weickmann, A. M.: High-resolution Doppler lidar for boundary layer and cloud research, J. Atmos. Ocean. Tech., 18, 376–393, https://doi.org/10.1175/1520-0426(2001)018<0376:HRDLFB>2.0.CO;2, 2001.

Hardesty, R. M. and Hoff, R. M.: Thermodynamic Profiling Technologies Workshop Report to the National Science Foundation and the National Weather Service, Tech. Rep. NCAR/TN-488+STR, National Center for Atmospheric Research, https://doi.org/10.5065/D6SQ8XCF, 2012.

Holden, J., Derbyshire, S., and Belcher, S.: Tethered balloon observations of the nocturnal stable boundary layer in a valley, Bound.-Lay. Meteorol., 97, 1–24, https://doi.org/10.1023/A:1002628924673, 2000.

Houston, A. L., Argrow, B., Elston, J., Lahowetz, J., Frew, E. W., and Kennedy, P. C.: The Collaborative Colorado–Nebraska Unmanned Aircraft System Experiment, Bulletin of the American Meteorological Society, 93, 39–54, https://doi.org/10.1175/2011BAMS3073.1, 2012.

Hubbard, K., Lin, X., Baker, C., and Sun, B.: Air temperature comparison between the MMTS and the USCRN temperature systems, J. Atmos. Ocean. Tech., 21, 1590–1597, https://doi.org/10.1175/1520-0426(2004)021<1590:ATCBTM>2.0.CO, 2004.

Kosiba, K., Wurman, J., Richardson, Y., Markowski, P., Robinson, P., and Marquis, J.: Genesis of the Goshen County, Wyoming, Tornado on 5 June 2009 during VORTEX2, Monthly Weather Review, 141, 1157–1181, https://doi.org/10.1175/MWR-D-12-00056.1, 2013.

Lackmann, G.: Midlatitude Synoptic Meteorology: Dynamics, Analysis, and Forecasting, American Meteorological Society, 2011.

Lanzante, J. R., Klein, S. A., and Seidel, D. J.: Temporal Homogenization of Monthly Radiosonde Temperature Data. Part I: Methodology, Journal of Climate, 16, 224–240, https://doi.org/10.1175/1520-0442(2003)016<0224:THOMRT>2.0.CO;2, 2003.

Lothon, M., Lohou, F., Pino, D., Couvreux, F., Pardyjak, E., Reuder, J., Vilà-Guerau De Arellano, J., Durand, P., Hartogensis, O., Legain, D., et al.: The BLLAST field experiment: boundary-layer late afternoon and sunset turbulence, Atmos. Chem. Phys., 14, 10 931–10 960, https://doi.org/10.5194/acp-14-10931-2014, 2014.

Luers, J. K. and Eskridge, R. E.: Use of Radiosonde Temperature Data in Climate Studies, Journal of Climate, 11, 1002–1019, https://doi.org/10.1175/1520-0442(1998)011<1002:UORTDI>2.0.CO;2, 1998.

Lundquist, J. K., Wilczak, J. M., Ashton, R., Bianco, L., Brewer, W. A., Choukulkar, A., Clifton, A., Debnath, M., Delgado, R., Friedrich, K., Gunter, S., Hamidi, A., Iungo, G. V., Kaushik, A., Kosović, B., Langan, P., Lass, A., Lavin, E., Lee, J. C.-Y., McCaffrey, K. L., Newsom, R. K., Noone, D. C., Oncley, S. P., Quelet, P. T., Sandberg, S. P., Schroeder, J. L., Shaw, W. J., Sparling, L., St. Martin, C., St. Pe, A., Strobach, E., Tay, K., Vanderwende, B. J., Weickmann, A., Wolfe, D., and Worsnop, R.: Assessing state-of-the-art capabilities for probing the atmospheric boundary layer: the XPIA field campaign, B. Am. Meteorol. Soc., 98, 289–314, https://doi.org/10.1175/BAMS-D-15-00151.1, 2017.

McPherson, R. A., Fiebrich, C. A., Crawford, K. C., Kilby, J. R., Grimsley, D. L., Martinez, J. E., Basara, J. B., Illston, B. G., Morris, D. A., Kloesel, K. A., Stadler, S. J., Melvin, A. D., Sutherland, A. J., Shrivastava, H., Carlson, J. D., Wolfinbarger, J. M., Bostic, J. P., and Demko,

D. B.: Statewide monitoring of the mesoscale environment: A technical update on the Oklahoma Mesonet, J. Atmos. Ocean. Tech., 24, 301–321, https://doi.org/10.1175/JTECH1976.1, 2007.

National Research Council: Observing weather and climate from the ground up: A nationwide network of networks, National Academies Press, 2009.

15 Neumann, P. P. and Bartholmai, M.: Real-time wind estimation on a micro unmanned aerial vehicle using its inertial measurement unit, Sensor Actuat. A-Phys., 235, 300–310, https://doi.org/10.1016/j.sna.2015.09.036, 2015.

Parker, M. D.: Composite VORTEX2 Supercell Environments from Near-Storm Soundings, Monthly Weather Review, 142, 508–529, https://doi.org/10.1175/MWR-D-13-00167.1, 2014.

Poulos, G. S., Blumen, W., Fritts, D. C., Lundquist, J. K., Sun, J., Burns, S. P., Nappo, C., Banta, R., Newsom, R., Cuxart, J., et al.: CASES-99:

20 A comprehensive investigation of the stable nocturnal boundary layer, B. Am. Meteorol. Soc., 83, 555–581, https://doi.org/10.1175/1520-0477(2002)083<0555:CACIOT>2.3.CO;2, 2002.

Reuder, J., Brisset, P., Jonassen, M., Müller, M., and Mayer, S.: The Small Unmanned Meteorological Observer SUMO: A new tool for atmospheric boundary layer research, Meteorologische Zeitschrift, 18, 141–147, 2009.

Reuder, J., Jonassen, M., and Ólafsson, H.: The Small Unmanned Meteorological Observer SUMO: Recent developments and applications

25 of a micro-UAS for atmospheric boundary layer research, Acta Geophys., 60, 1454–1473, https://doi.org/10.2478/s11600-012-0042-8, 2012.

Richardson, S. J., Brock, F. V., Semmer, S. R., and Jirak, C.: Minimizing errors associated with multiplate radiation shields, J. Atmos. Ocean. Tech., 16, 1862–1872, https://doi.org/10.1175/1520-0426(1999)016<1862:MEAWMR>2.0.CO;2, 1999.

Rodert, L. A.: The Effects of Aerodynamic Heating on Ice Formations on Airplane Propellers, Technical Report 799, National Advisory

30 Committee for Aeronautics, Langley Aeronautical Lab, https://ntrs.nasa.gov/search.jsp?R=19930081671, 1941.

Saïd, F., Corsmeier, U., Kalthoff, N., Kottmeier, C., Lothon, M., Wieser, A., Hofherr, T., and Perros, P.: ESCOMPTE experiment: intercomparison of four aircraft dynamical, thermodynamical, radiation and chemical measurements, Atmos. Res., 74, 217–252, https://doi.org/10.1016/j.atmosres.2004.06.012, 2005.

Seidel, D. J., Ao, C. O., and Li, K.: Estimating climatological planetary boundary layer heights from radiosonde observations: Comparison

35 of methods and uncertainty analysis, J. Geophys. Res.-Atmos., 115, https://doi.org/10.1029/2009JD013680, 2010.

Shapiro, M. A.: Meteorological tower measurements of a surface cold front, Mon. Weather Rev., 112, 1634–1639, https://doi.org/10.1175/1520-0493(1984)112<1634:MTMOAS>2.0.CO;2, 1984.

Stull, R.: An Introduction to Boundary Layer Meteorology, Dordrecht, 9 edn., 1988.

Swean, T. F. and Schetz, J. A.: Flow about a Propeller-Driven Body in Temperature-Stratified Fluid, AIAA J., 17, 863–869, https://doi.org/10.2514/3.61238, 1979.

5 Tanner, B. D., Swiatek, E., and Maughan, C.: Field comparisons of naturally ventilated and aspirated radiation shields for weather station air temperature measurements, vol. 22, pp. 227–230, Conference on Agricultural and Forest Meteorology, 1996.

Thompson, D. W. J. and Solomon, S.: Recent Stratospheric Climate Trends as Evidenced in Radiosonde Data: Global Structure and Tropospheric Linkages, Journal of Climate, 18, 4785–4795, https://doi.org/10.1175/JCLI3585.1, 2005.

Toms, B. A., Tomaszewski, J. M., Turner, D. D., and Koch, S. E.: Analysis of a Lower-Tropospheric Gravity Wave Train Using Direct and

10 Remote Sensing Measurement Systems, Monthly Weather Review, 145, 2791–2812, https://doi.org/10.1175/MWR-D-16-0216.1, 2017.

Trapp, R. J., Stensrud, D. J., Coniglio, M. C., Schumacher, R. S., Baldwin, M. E., Waugh, S., and Conlee, D. T.: Mobile Radiosonde Deployments during the Mesoscale Predictability Experiment (MPEX): Rapid and Adaptive Sampling of Upscale Convective Feedbacks, Bulletin of the American Meteorological Society, 97, 329–336, https://doi.org/10.1175/BAMS-D-14-00258.1, 2016.

van den Kroonenberg, A. C., Martin, S., Beyrich, F., and Bange, J.: Spatially-averaged temperature structure parameter over a heterogeneous surface measured by an unmanned aerial vehicle, Bound.-Lay. Meteorol., 142, 55–77, https://doi.org/10.1007/s10546-011-9662-9, 2012.

460 Vömel, H., Argrow, B. M., Axisa, D., Chilson, P., Ellis, S., Fladeland, M., Frew, E. W., Jacob, J., Lord, M., Moore, J., Oncley, S., Roberts, G., Schoenung, S., and Wolff, C.: The NCAR / EOL Community Workshop on Unmanned Aircraft Systems for Atmospheric Research, UCAR/NCAR Earth Observing Laboratory, https://doi.org/10.5065/D6X9292S, 2018.

Waugh, S. and Fredrickson, S.: An improved aspirated temperature system for mobile meteorological observations, especially in severe weather, *25th Conf. on Severe Local Storms*, Denver, CO, Amer. Meteor. Soc., P5.2., 2010.

465 Wildmann, N., Hofsäß, M., Weimer, F., Joos, A., and Bange, J.: MASC-a small remotely piloted aircraft (RPA) for wind energy research, Adv. Sci. Res., 11, 55, https://doi.org/10.5194/asr-11-55-2014, 2014.

24